SS-146
2251

NEUTRINO BEAM DESIGN

Y. W. Kang and F. A. Nezrick
National Accelerator Laboratory

ABSTRACT

The important parameters of neutrino beams have been studied at NAL to develop a conceptual neutrino beam design. It has been found that a neutrino beam with a decay length of 600 m, a shielding thickness of 300 m, and a decay tunnel radius of 0.75 m is quite appropriate for either 200-BeV or 400-BeV operation of the NAL proton synchrotron. It appears useful to fill the decay tunnel with bags of He or operate in vacuum to substantially reduce the number of secondary beam (π or K) collisions in the decay tunnel. With a focusing system of two elements located inside target station T1, one elastic event in every four pictures of the 25 ft deuterium-filled bubble chamber can be obtained.

INTRODUCTION

The important parameters in a neutrino beam design have been investigated by using a computer program[1] so that a conceptual neutrino beam for NAL could be developed.[2] For the conceptual design work, the CKP particle production formula with $K/\pi = 0.15$ has been used. Later in the more detailed design calculations, other particle production formula will be investigated. The π and K mesons with momenta from 7.5 BeV to 157.5 BeV within a maximum production angle of 60 mrad have been used in the calculations. A detector radius of 1.8 m and shielding thickness of 600 m, 150 m, and 70 m for earth, iron, and uranium, respectively, were assumed.

A series of detailed calculations was performed to study the following problems:

1. The variation of neutrino flux with decay length for perfect focusing and different shielding materials, earth, iron, and uranium. The effects are illustrated in Figs. 1-4.

2. The neutrino energy spectra for the three optimized geometries using the best decay length for each shielding thickness. (Perfect focusing.) See Figs. 5 and 6.

3. The dependence of the neutrino flux on the detector radius. (Perfect, real, and no focusing). See Figs. 7-15.

4. The dependence of the neutrino flux on the decay tunnel radius. (Real focusing and no focusing.) See Figs. 16-18.

5. The neutrino energy spectra for the iron-shielded beam. (Perfect, real, and no focusing.) See Fig. 19.

6. The dependence of neutrino flux on the number of focusing elements. (Real focusing.) See Fig. 20.

7. Extension to 400 BeV: the dependence of neutrino flux on the decay length for the iron-shielded beam. (Perfect focusing.) See Figs. 21 and 22.

8. Optimization of the locations and currents for a three-element focusing system. See Fig. 23.

9. Improvement in real focusing by meson ray traces.

10. The neutrino flux using a thick target. See Fig. 24.

11. Neutrino energy spectra for specific pion and kaon momenta. See Fig. 25.

12. Energy hardening of the neutrino beam.

13. Neutrino event rate in a deuterium bubble chamber.

A detailed discussion of each set of calculations will be given below.

DETAILED CALCULATIONS

1. The neutrino-flux dependence on decay length for different shield materials--earth, iron, and uranium. (Perfect focusing.)

For the assumed shield thicknesses of 600 m for earth, 150 m for iron, and 70 m for uranium, the integrated neutrino fluxes passing through the detector were calculated for different decay lengths. The integrated neutrino fluxes above different energies for the different shields are given in Figs. 1 and 2 for pion and kaon decays respectively as a function of decay length. The maximum production angle allowed was 20 mrad. The flux variation with decay distances can be understood by recalling that the mean decay distances for the pion and kaon are 55 m/BeV/c and 7.5 m/BeV/c, respectively. In general, then, the integrated flux of neutrinos from the pion decays slowly increases with increasing decay length, while the integrated flux from the kaon decays decreases with decay length because of the solid angle factor.

For pion neutrinos, the integrated flux above 6 BeV for the iron-shield beam is about three times as large as that from the earth-shielded beam with a decay length of 600 m. The flux from the iron-shielded beam is only about 30% inferior to that from the uranium-shielded beam.

For the iron-shielded beam, the neutrino flux produced from kaon decays becomes comparable to that produced from pion decays for neutrino energies above about 25 BeV, at a decay length of 600 m. The kaon neutrino flux above 35 BeV for an

iron-shielded beam is about three times greater than that from the earth-shielded beam, while it is about 30% inferior to that for the uranium-shielded beam.

The integrated neutrino flux from π and K decays passing through the detector as a function of decay distance is given in Fig. 3 for neutrino energies above 2.5 BeV and 40 BeV. Under the assumptions of the calculations an optimized decay length can be obtained from Fig. 3 for each shield thickness, and is given in Fig. 4 for the integrated flux above 2.5 BeV. The optimal decay length increases with shielding thickness but its choice is not critical because of the flatness of the integrated flux curves in Fig. 3. For our purposes a decay length of 600 m has been chosen because it produces a neutrino flux which is within 10% of being optimal for both high and low energy neutrinos.

2. The energy spectra for the three different muon-shielded beams with optimized decay lengths. (Perfect focusing.)

Using the optimum decay lengths from Fig. 4 for the shields of uranium, iron and earth, the energy distribution of the neutrinos passing through the detector was calculated and is shown in Fig. 5. The iron-shielded beam is inferior to the uranium-shielded beam in the energy regions below 7 BeV and around 30 BeV, while it is far superior to the earth-shielded beam below 15 BeV.

The solutions presented in Fig. 5 use a maximum allowed production angle of 20 mrad. A slightly different set of decay lengths better illustrate the effect of the shield thickness on the neutrino energy distribution. For a maximum allowed production angle of 60 mrad, Fig. 6 gives the neutrino energy distribution for three different shield thicknesses for a fixed decay length and for the earth-shielded beam. For the fixed decay length one observes that as the shield thickness is increased one loses the neutrinos from the low energy pion and kaon decays while the neutrino flux from the higher energy pion decays remain essentially constant. If the decay length and shield thickness are both increased, then the neutrino flux contribution is reduced from the kaon decays and from the low energy pion decays but is increased from the higher energy pion decays. This is as expected from the ratio of the particle mean decay length to the length of the decay region.

3. The variation of the neutrino energy distribution with the detector radius. (Perfect, real, and no focusing.)

Using the iron-shielded beam with a 600 m decay length, the neutrino fluxes have been determined for different distances from the neutrino beam axis at the detector. We present nine graphs which give the radial dependence of the neutrino flux resulting from pion decays, from kaon decays, and from pion plus kaon decays, for perfect (Figs. 7-9), real (Figs. 10-12), and no focusing (Figs. 13-15), respectively.

First consider the perfectly-focused case for pions, Fig. 7, for kaons, Fig. 8, and for pions plus kaons, Fig. 9. The general properties of these distributions can be roughly understood by considering the 6-BeV neutrino distribution from perfectly-focused pions, Fig. 7. The flux per unit area has a maximum at about 1.5 m radius and it decreases for larger and smaller detector radii. These decreases reflect an interplay of the pion decay kinematics and the range of decay distances from the detector. For example, consider the decay of 20-BeV pions to give 6-BeV neutrinos, which are copiously produced. The neutrino decay angle is 3.5 mrad so that the trajectory passes through the detector at radial distances from 3.1 m to 1.0 m depending on whether the pion decayed at the beginning or the end of the 600-m long decay region. In other words, fixed-energy neutrinos from a fixed-energy pion decay pass through a sharply defined radial band at the detector. The inside and outside radii of this region at the detector are determined by the shortest and longest pion decay distance from the detector. The distributions of Fig. 7 do not have sharp limits because a spectrum of neutrinos is produced from a fixed-energy pion decay and decreases logarithmically with increasing energy.

From Fig. 7 we see that the pion neutrinos start to show a focused behavior at about 12 BeV while from Fig. 8 the kaon neutrinos start showing a focused behavior at about 40 BeV. Combining the contributions of pion and kaon decays gives the distributions shown in Fig. 9. The neutrino flux between 30 BeV and 40 BeV shows rather unusual variations when the kaon contribution is included.

Using real focusing elements we obtain Figs. 10-12. The no-focusing case produces the distributions given on Figs. 13-15. The no-focusing distributions are rather flat around the center of the detector and fall off slowly. By comparing Figs. 12 and 15 the advantages and quality of focusing are apparent.

4. The neutrino flux dependence on decay tunnel diameter. (Real and no focusing).

From Figs. 16-18 we see that a maximum useful decay tunnel diameter is 4 m for a non-focused beam and 3 m for a real focused beam, to optimize the flux in a detector 3.6 m in diameter. Making the tunnel radius a function of the distance from the target was also investigated. It was found that the decay tunnel could be appreciably reduced near the shield without a noticable flux loss. A tunnel diameter of 1.5 m reduces the flux at the detector by only 30%, but gives a considerable reduction of the transverse size of the muon shield.

5. The neutrino energy spectrum for the iron-shielded beam. (Perfect, real and no focusing.)

In Fig. 19 we show a comparison of neutrino fluxes for the perfect, real- and no-focusing cases. The real focusing calculation includes absorption in the horn material and target, while the perfect focusing includes only absorption in the target. On the average the real focusing is about 75% of perfect focusing. The maximum production angle accepted was 20 mrad in the calculation.

6. The neutrino flux dependence on the number of the focusing elements.

A neutrino beam focusing system of three elements has been studied. A preliminary design of the first focusing element was made and the efficiency of the second and third elements was studied. From Fig. 20, the two-element system is only 5% poorer than the three-element system, while the one-element system is 50% efficient. The first two focusing elements are located inside the target station, while the third element could be outside. During the first stages of the neutrino program at NAL a two-element system should be completely adequate.

7. Extension to 400 BeV: the flux dependence on decay length for the iron-shielded beam. (Perfect focusing.)

The 200-BeV accelerator will be extended to 400 BeV after several years' operation. We hope to extend the neutrino beam to 400 BeV with minimum modifications. Our main concern is not to change the location of the large bubble chamber, the muon shield, and the target station.

We see in Fig. 21 that the optimum decay length would be 1,000 m but 600 m is also quite reasonable because of the broadness of the optimum. Figure 22 gives the dependences for the pion and kaon decays individually. With the decay length of 600 m, we have a high-energy flux (> 50 BeV) comparable to that at 1,000 m. Hence the selection of 600 m is quite adequate because we suppose that the higher energy neutrinos will be more important than the low energy neutrinos when 400 BeV protons are available.

Therefore, the decay length of 600 m has been chosen in both 200 BeV and 400 BeV operations. The neutrino flux increase over the 200 BeV case is about a factor of two, as we expect.

8. Optimization of the locations and currents of the last two focusing elements.

For focusing elements of a given shape we can find the best positions and current for the last two elements to maximize the neutrino flux passing through the detector. Assuming the first element current, we calculated the neutrino flux as a function of the second element location and current. By a process of iteration we obtain the best values for the second element position and current. For a three-element system we proceeded in a similar way after we had fixed the location and current of the second element. However, we have not investigated the three-element system by optimizing

simultaneously the currents in the three elements and the position of the second and third elements. The best parameters of the elements shown in Fig. 23 were determined and are given in Table I.

Table I. Optimal Positions and Currents for Focusing Elements.

	First Element	Second Element	Third Element
Distance from target (m)	0	50	200
Current of focusing element (MA)	0.3	0.4	0.3

9. Efficiency improvement in real focusing by ray traces.

Up to this point the focusing system and flux distributions have been calculated without knowing in detail the individual pion and kaon trajectories in the decay tunnel. We have also studied by ray traces how the individual particles with given momenta and production angles behave throughout the focusing system. The study of ray traces gives some idea of how the shape of the inner conductor of a focusing element should be modified to improve a particular momentum region at a particular production angle. By repeating ray traces and optimization of the focusing element parameters alternatively, we can improve the focusing systems.

10. The neutrino flux from a thick target.

We have calculated a neutrino flux efficiency as a function of position along the target and found that the flux was fairly uniform along the 2.5 m long target region. (See Fig. 23.) We also calculated the fluxes for short and long targets (0.45 m long Cu and 2.5 m long Li target with the same radii of 2 mm). The Li target is better in the flux yield by 15% than Cu target. A flux distribution for a 2.5 m long thick target is given in Fig. 24 and will be used for the estimate of a neutrino event rate.

11. The neutrino energy spectra for given pion or kaon momenta.

In Fig. 25, we give the neutrino energy spectra passing through the detector for fixed pion or kaon momenta calculated for the real focusing case. The energy spectra taper off at the lower and higher energy ends. If we had 4π acceptance by the focusing elements, we would observe a rectangular spectrum.

12. The energy hardening of the neutrino beam.

In some experiments, only the high energy neutrinos (greater than 40 BeV), are desirable while the interactions of low energy neutrinos (less than 40 BeV) are regarded as background. In general, the low energy pions or kaons are very sensitive to the focusing in the first element. With this aim in mind, we have calculated fluxes by changing the current signs of two elements with respect to the first. For one

focusing and two defocusing elements, for example, the high energy neutrinos are reduced by a factor of two while the low energy neutrinos are reduced by a factor of four. The focusing effect on the oppositely charged particles is found to be negligible. This was a very preliminary investigation but looks promising. Hardening can also be accomplished by not using the first focusing element. Further improvement will be investigated by current variations and modifying the inner conductor shapes.

13. Neutrino elastic event rate.

A neutrino event rate in the 25-ft deuterium bubble chamber is determined on the basis of the flux yield shown in Fig 24. The 25-ft bubble chamber will have a usable fiducial volume of 70,000 liters with an approximate 7 m length. Since the inelastic cross section is less well known at present, only the elastic events will be considered with an assumed cross section of 10^{-38} cm^2. The actual event rate is expected to be much greater than we estimate here because of a large neglected inelastic event rate. The 200-BeV proton intensity is 5×10^{13} protons/pulse. The event rate is about one event every four pictures. In this estimate we included the attenuation effect in the decay tunnel (filled with bags of He), absorption effect in the focusing elements and the target, the target efficiency and also the reduction due to the tunnel radius being 0.75 m. A K to π ratio of 10 percent was assumed. A further detail of the events in different energy regions is given in Table II.

Table II. Origin of Neutrino Spectral Distribution.

Neutrino Energy (BeV)	2.5-10	10-40	40-100
Pion (%)	80	20	-
Kaon (%)	-	70	30
Total (%)	78.9	20.6	0.5

CONCLUSIONS

We have calculated the important parameters for a conceptual neutrino beam at NAL. The parameters of the neutrino beam design follow:

1. The decay length: 600 m

2. The muon shielding thickness: 100 m of iron plus 200 m of earth under the 200-BeV operation and 300 m of iron shielding under the 400-BeV operation.

3. The radius of the decay tunnel: 0.75 m.

4. The above parameters do not change in going from 200-BeV to 400-BeV operation. The positions of the target station, the beginning of the muon shielding, and the bubble chamber do not change.

5. During the first stage of the neutrino program, we will use a two-element focusing system which is located inside the target station.

6. When including the absorption effects in the focusing elements, the absorption in the target, the target efficiency, the attenuation effect in the decay tunnel, the efficiency of a two-element focusing system, and the reduction due to the tunnel radius being 0.75 m, the elastic event rate is estimated to be one event in every four pictures of the 25-ft deuterium-filled bubble chamber.

REFERENCES

[1]This report was originally written as Appendix IX of Research Facilities Design Concepts--Summer 1969, National Accelerator Laboratory Internal Report TM-181, May-June 1969. In the original report a few of the calculations for the non-focused cases were incorrect because of angle quantization problems in the computer coding. These problems have been overcome and the corrected figures are presented in this report.

[2]The neutrino flux program used at NAL is a variation of the CERN program. We wish to thank Dr. W. Venus for the private communication of the CERN program.

Note: Unless otherwise indicated, the target thickness is 0.033 interaction lengths (1 cm) long. When the flux is dimensionless, it is to be considered as a relative flux.

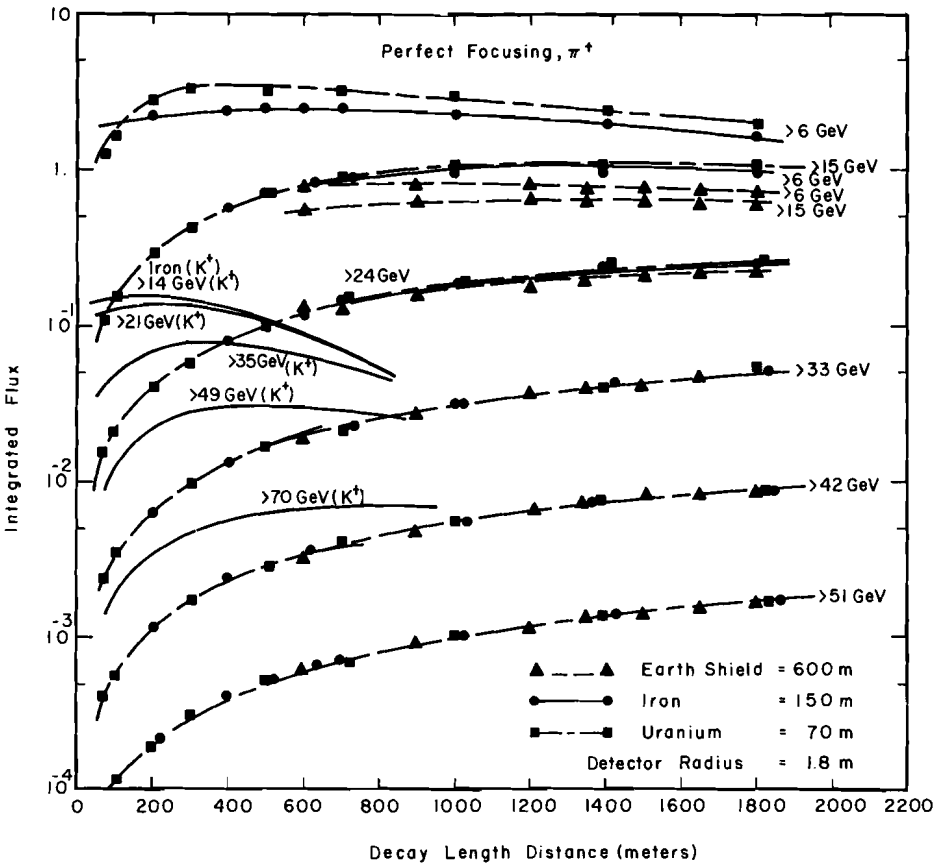

Fig. 1. The dependence of the integrated neutrino flux from pion decays on the decay length for different shield thicknesses. The flux from kaon decays (an iron shield) are given for comparison.

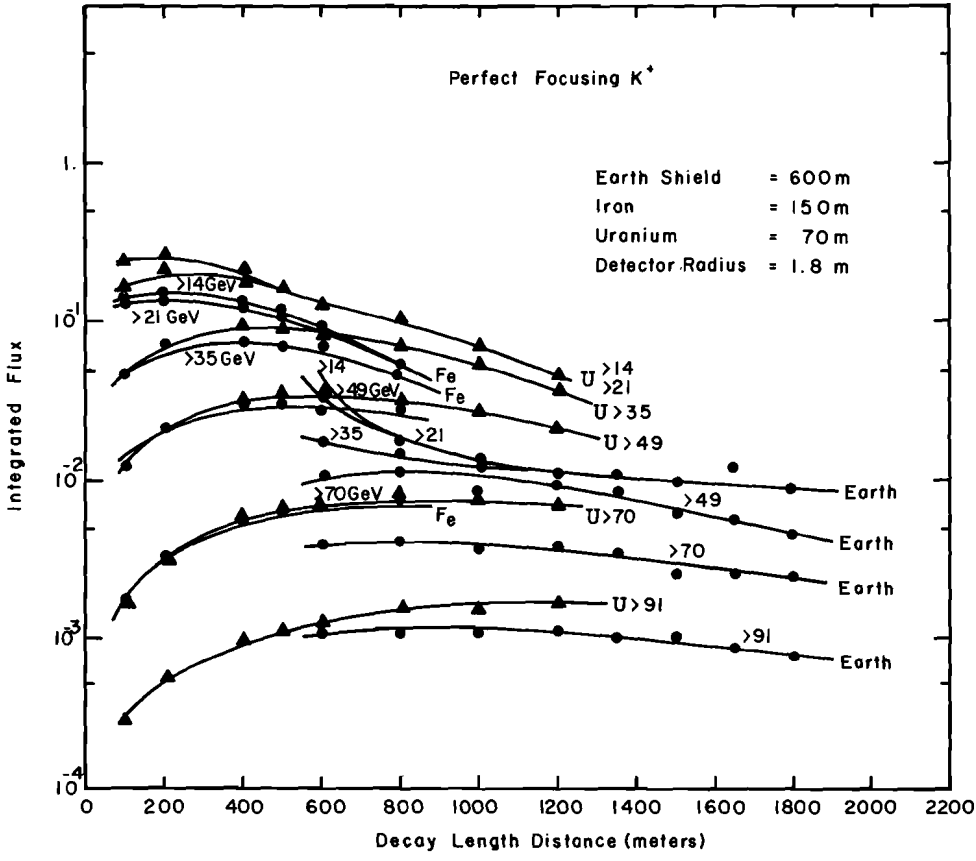

Fig. 2. The dependence of the integrated neutrino flux from kaon decays on the decay length for different shield thicknesses.

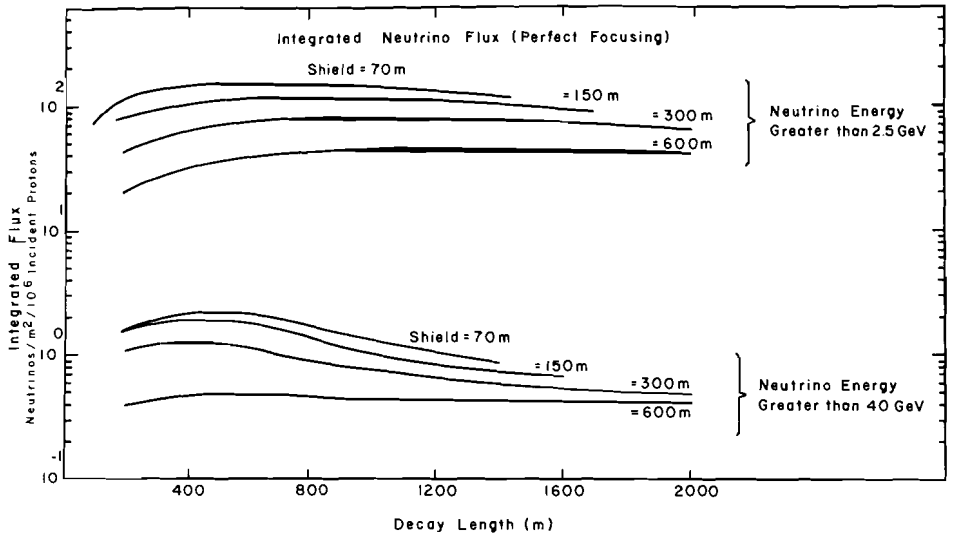

Fig. 3. The dependence of the integrated neutrino flux from kaon decays on the decay length for different shield thicknesses.

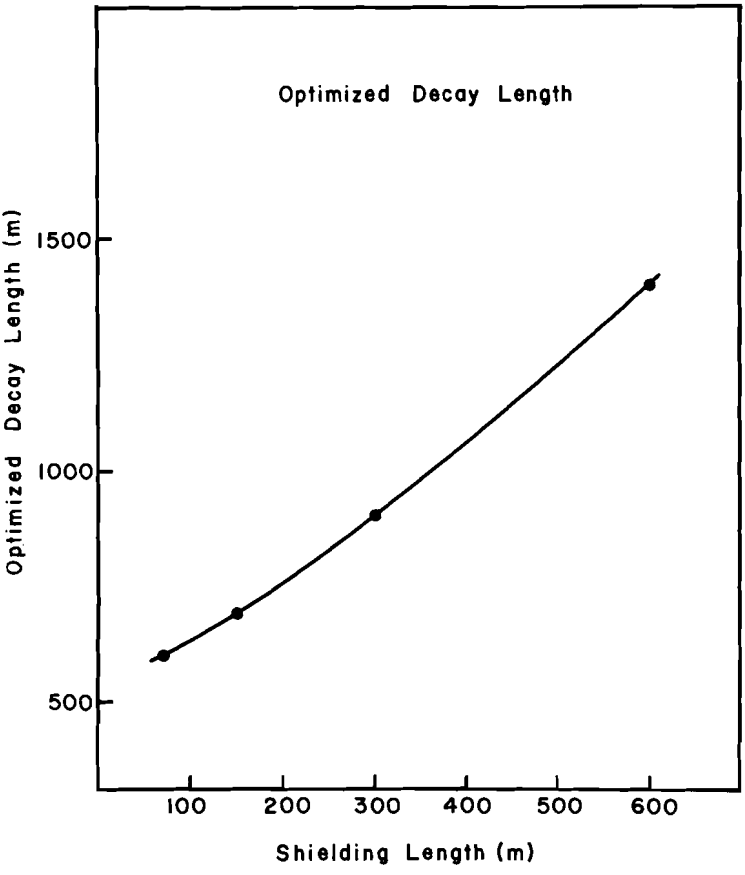

Fig. 4. The dependence of the optimized decay length on the shield thickness.

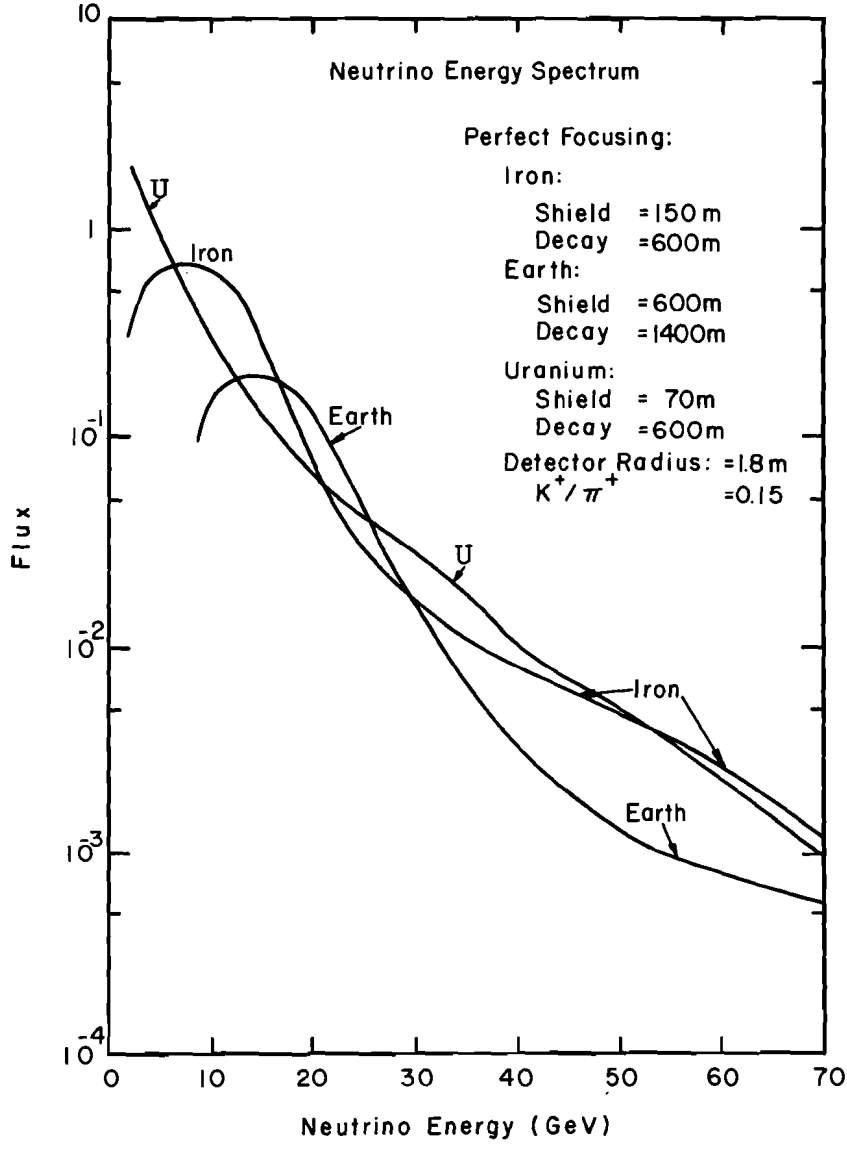

Fig. 5. Neutrino energy spectra from beams composed of uranium, iron or earth shields, and their respective optimized decay lengths.

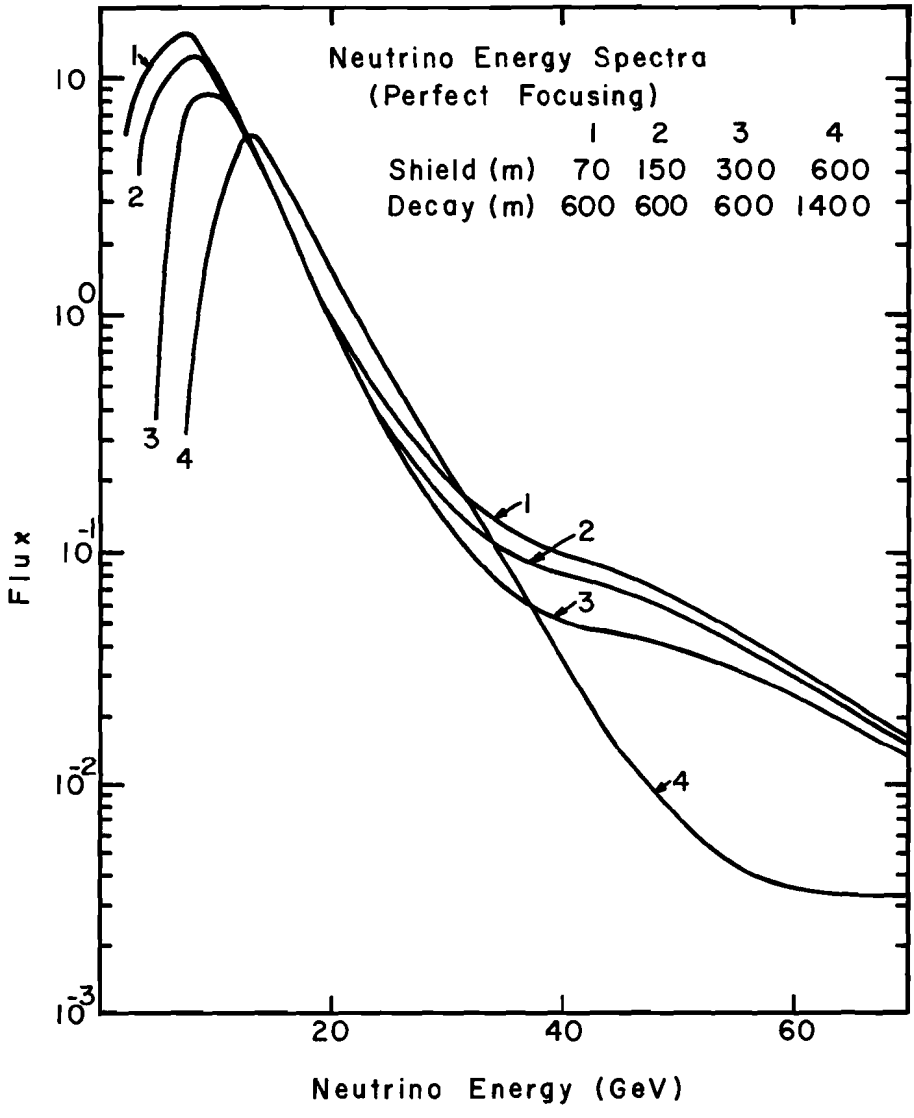

Fig. 6. Neutrino energy spectra from four beams of different shield-decay length combinations.

Figs. 7-15. These figures present the radial distribution of fixed energy neutrinos at the detector. The beam used was a decay length of 600 m and an iron-shield thickness of 150 m. The figures present the distributions from the decays of different parents in different focused beams.

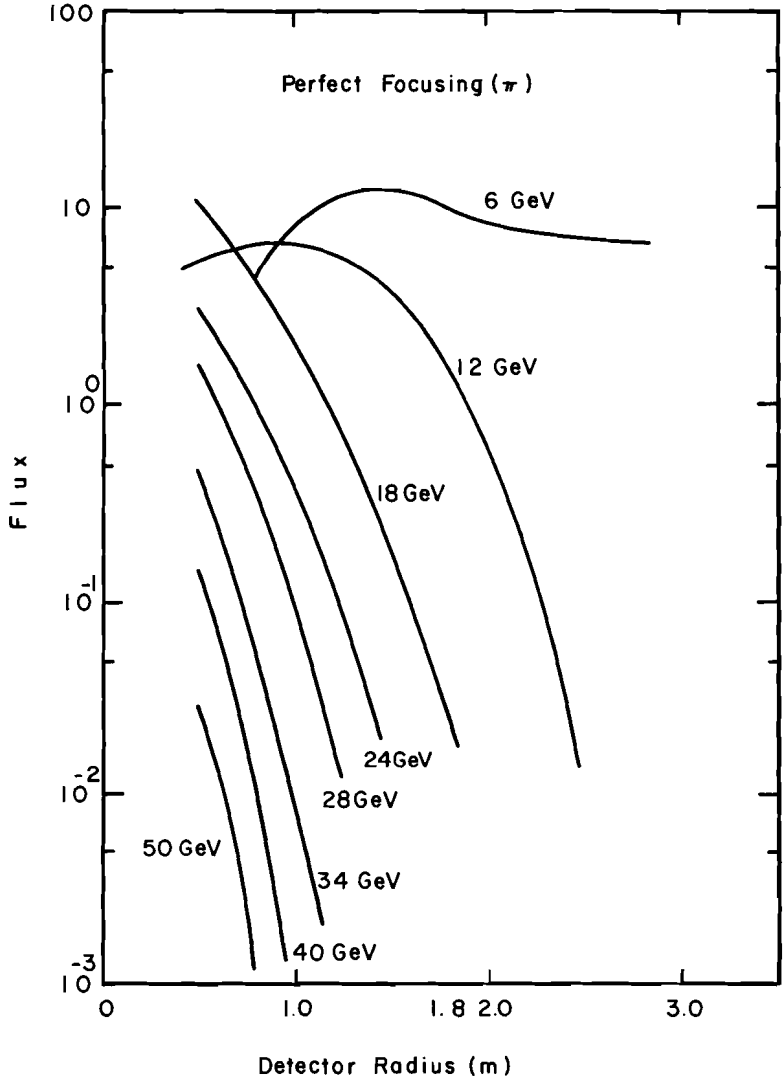

Fig. 7. Parents: π. Parent focusing: perfect focusing.

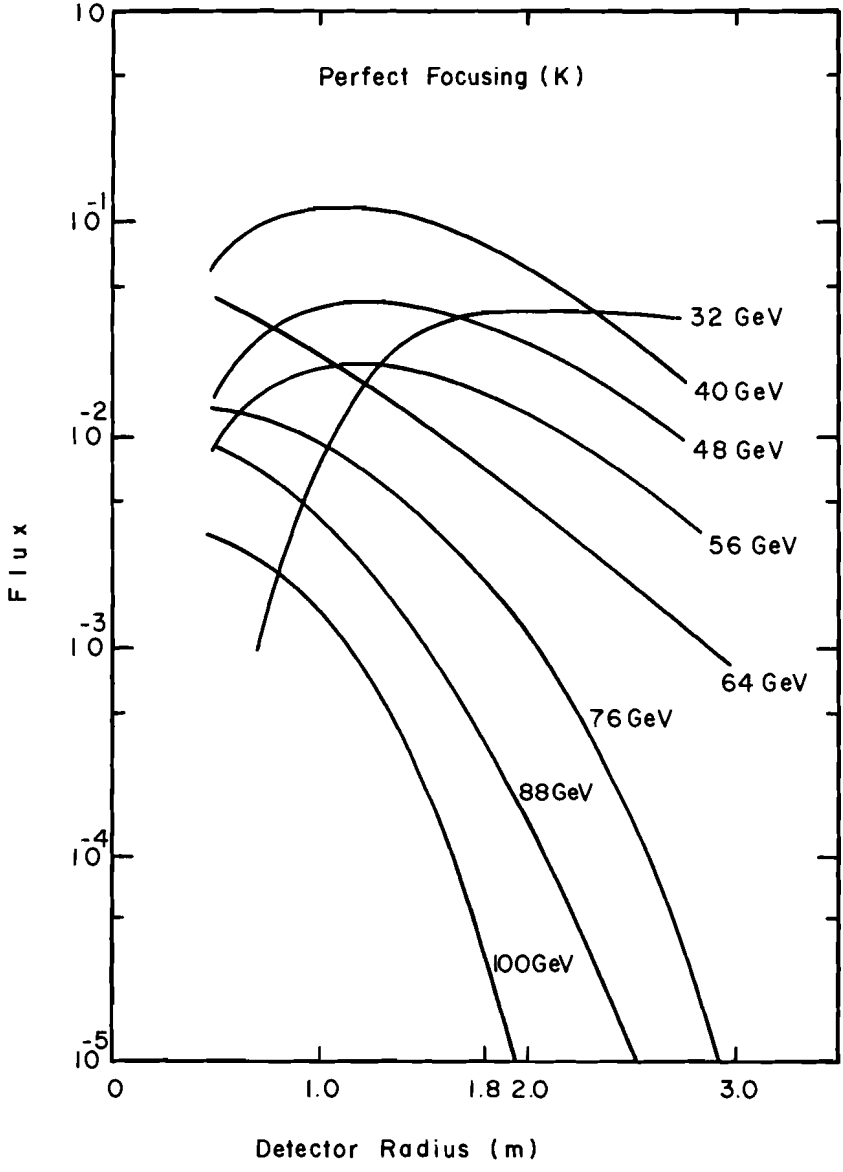

Fig. 8. Parents: K. Parent focusing: perfect focusing.

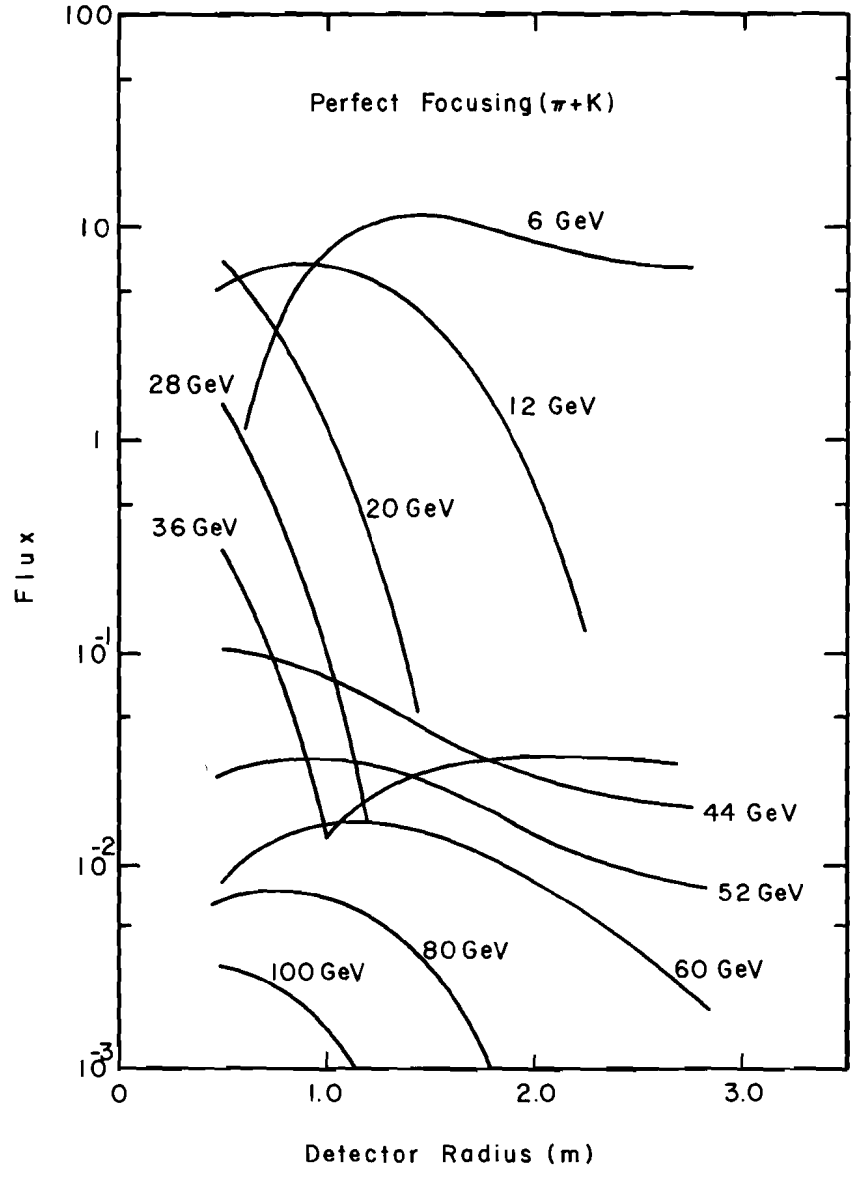

Fig. 9. Parents: π+K. Parent focusing: perfect focusing.

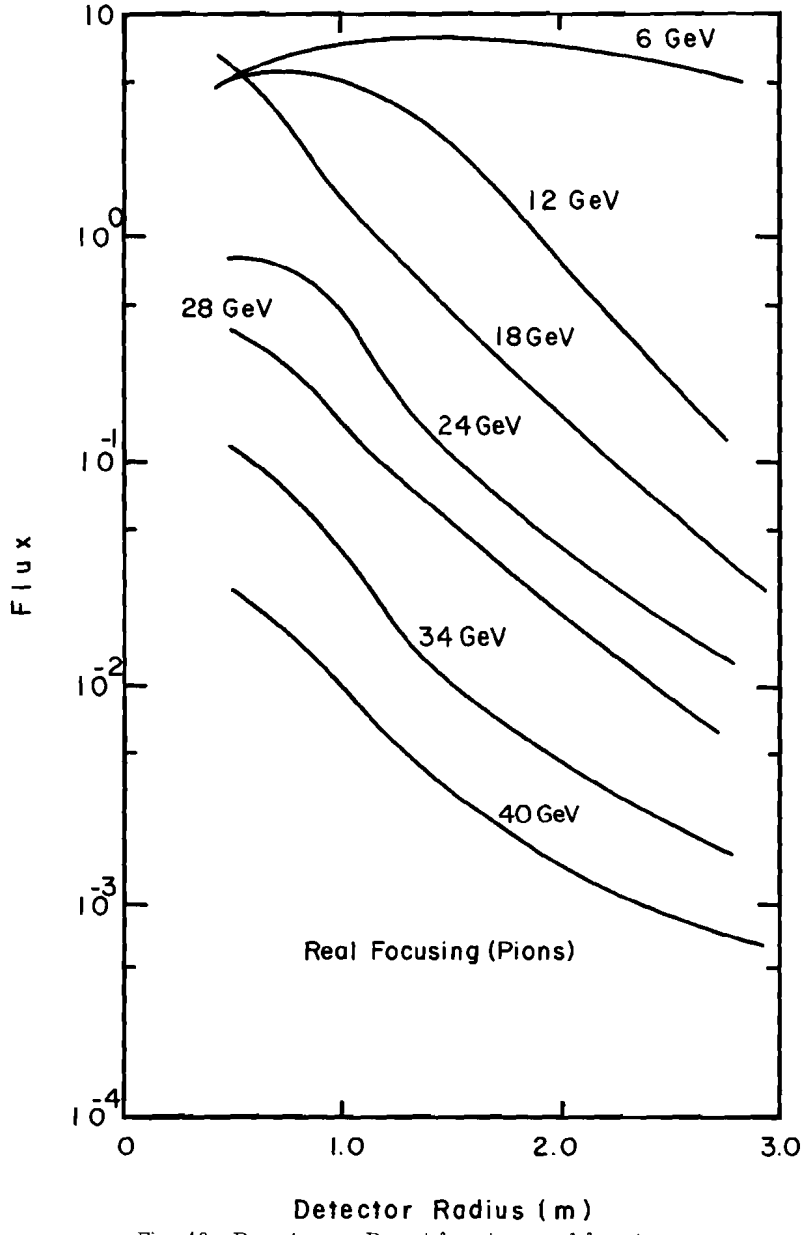

Fig. 10. Parents: π. Parent focusing: real focusing.

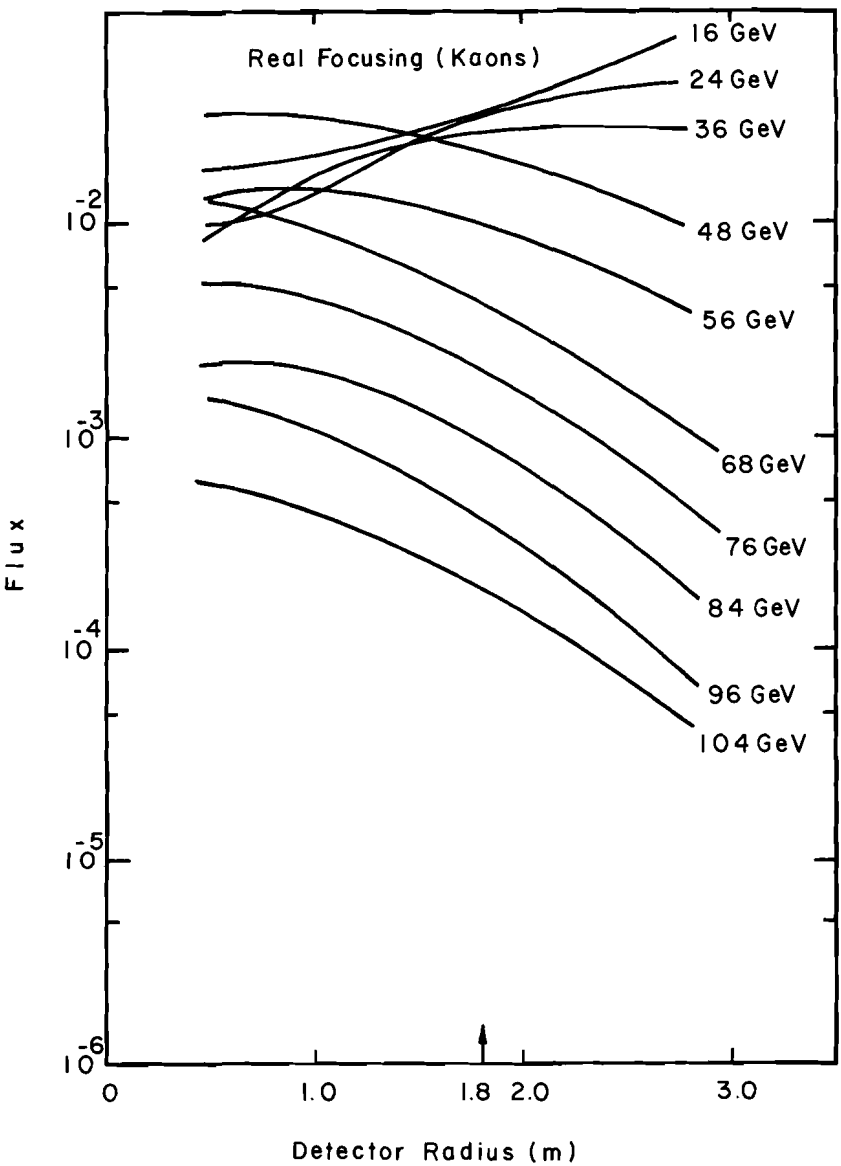

Fig. 11. Parents: K. Parent focusing: real focusing.

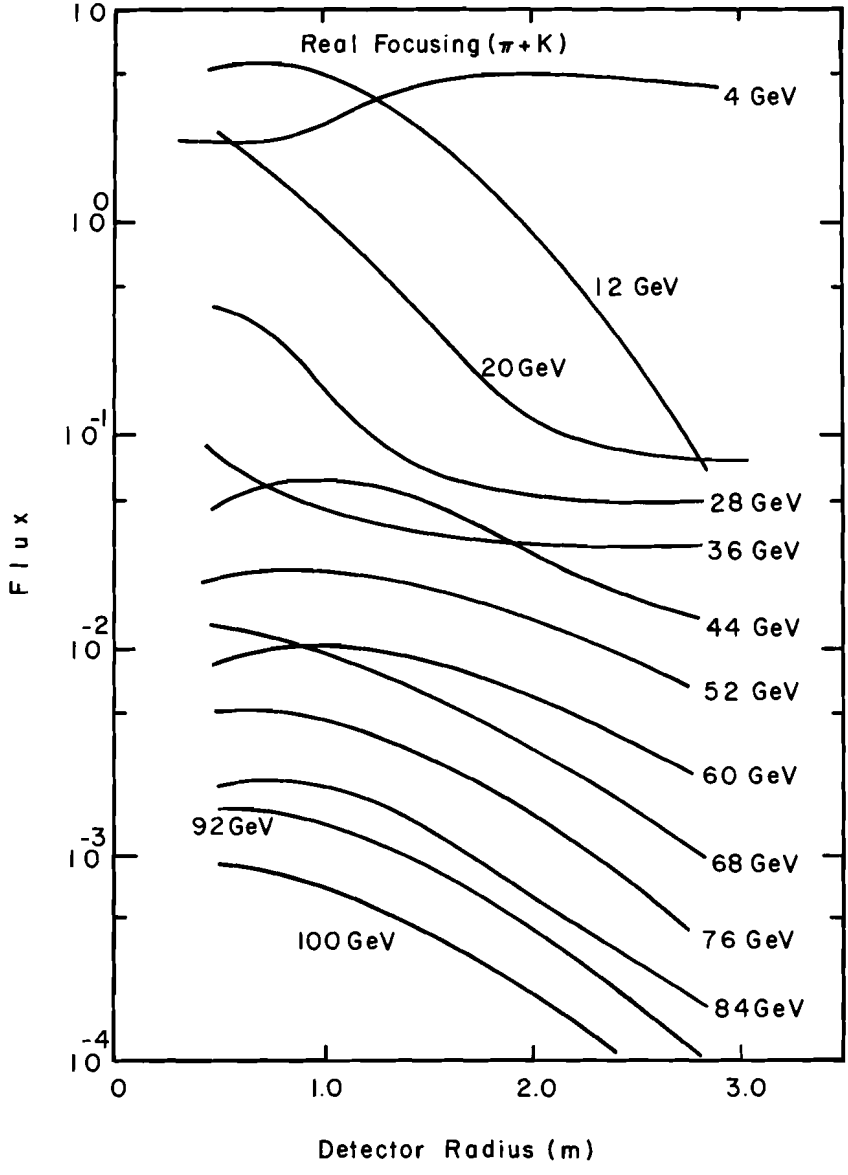

Fig. 12. Parents: π + K. Parent focusing: real focusing.

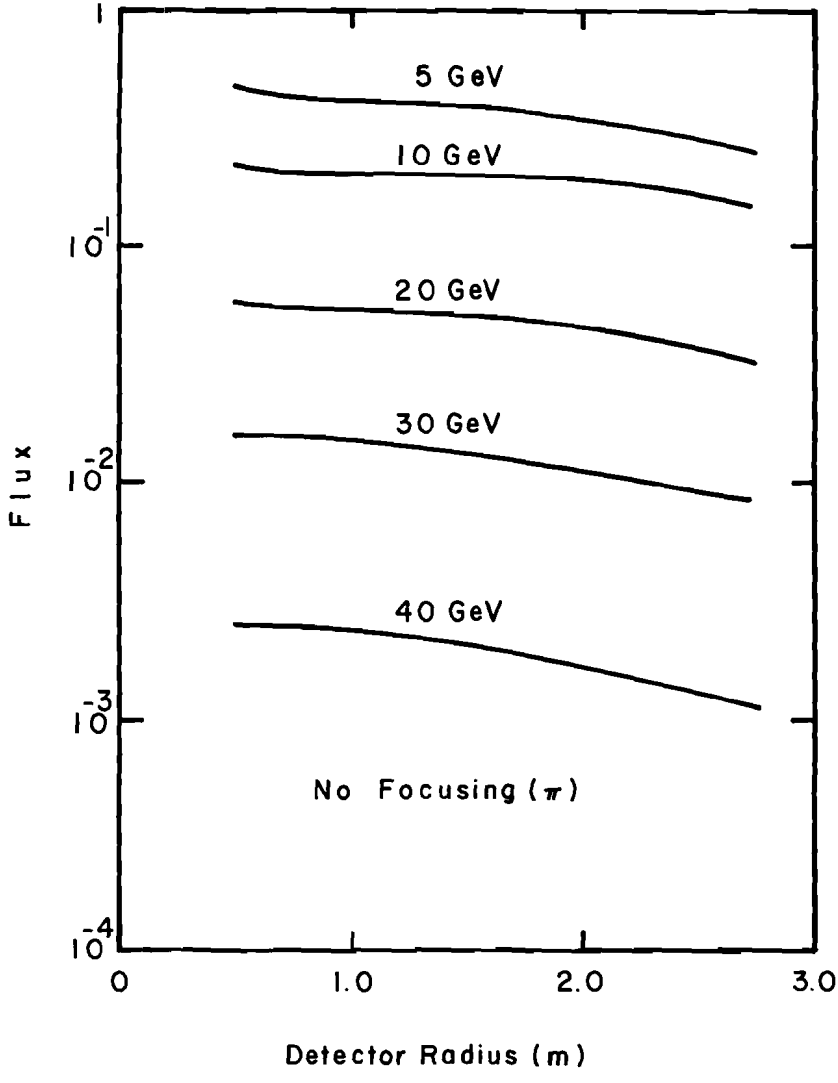

Fig. 13. Parents: π. Parent focusing: no focusing.

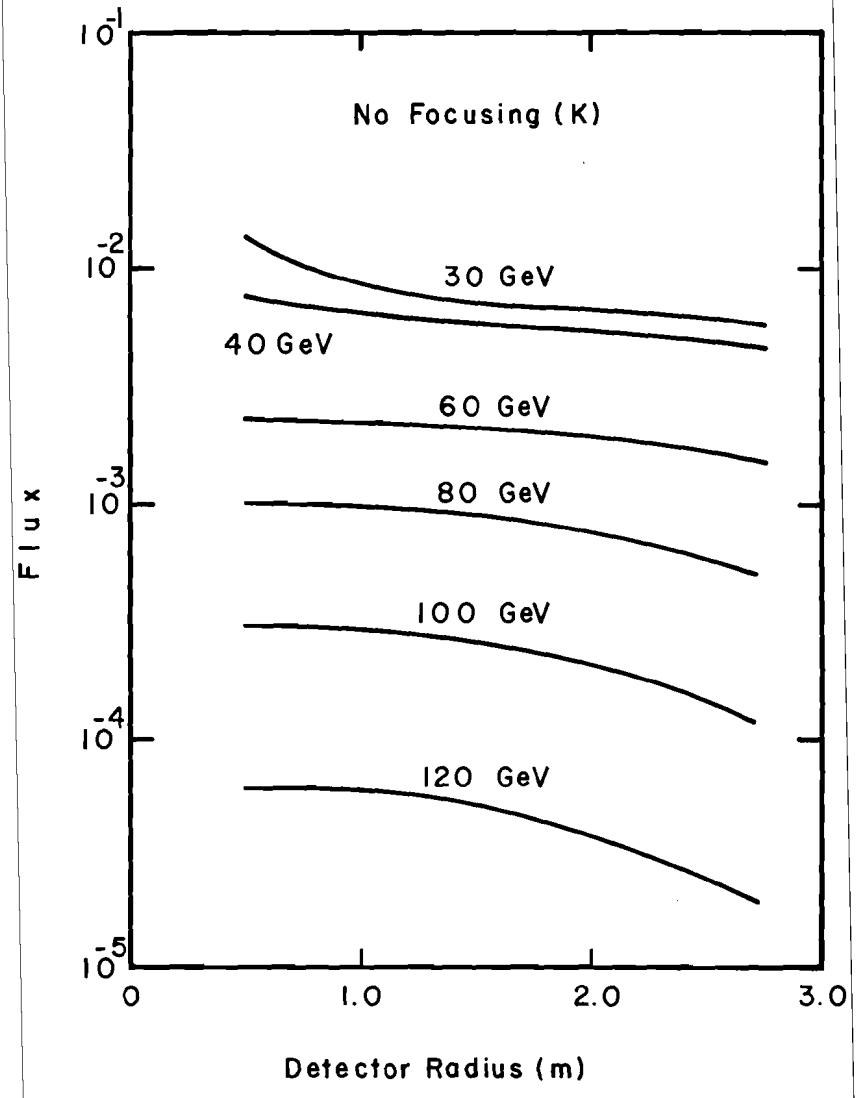

Fig. 14. Parents: K. Parent focusing: no focusing.

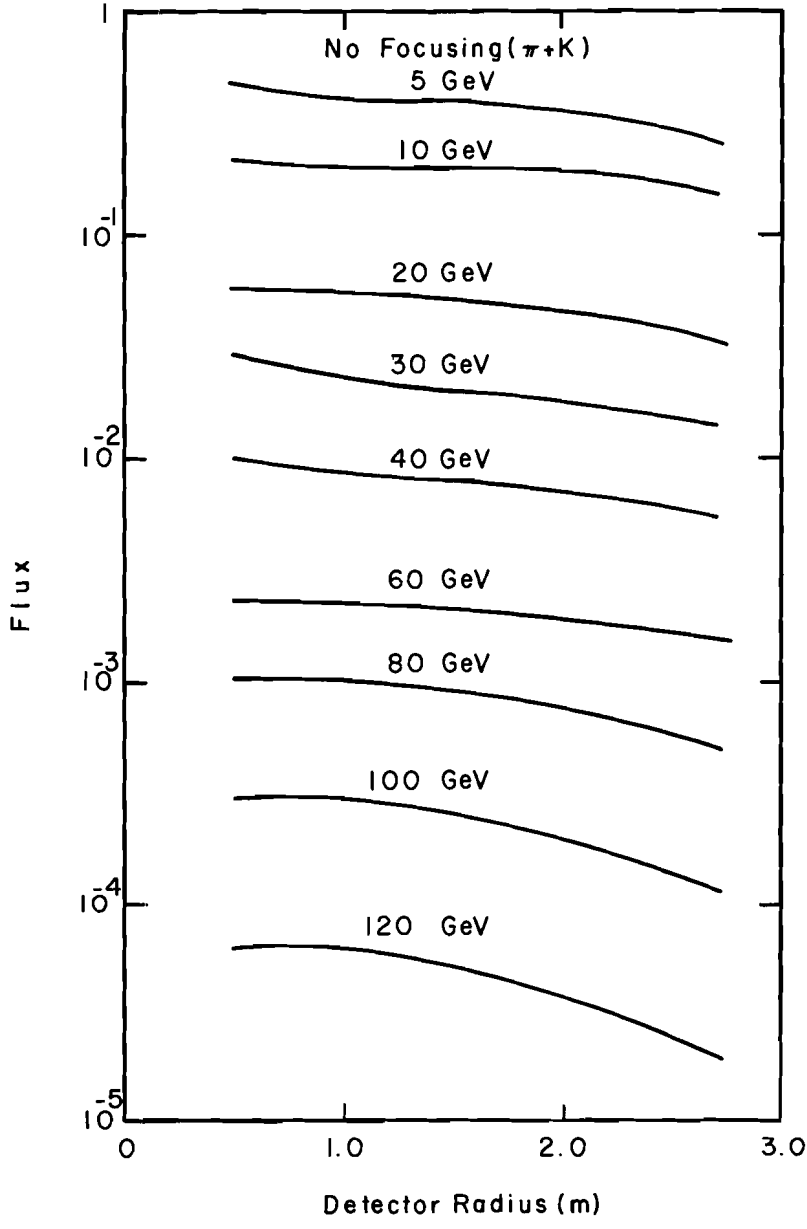

Fig. 15. Parents: $\pi + K$. Parent focusing: no focusing.

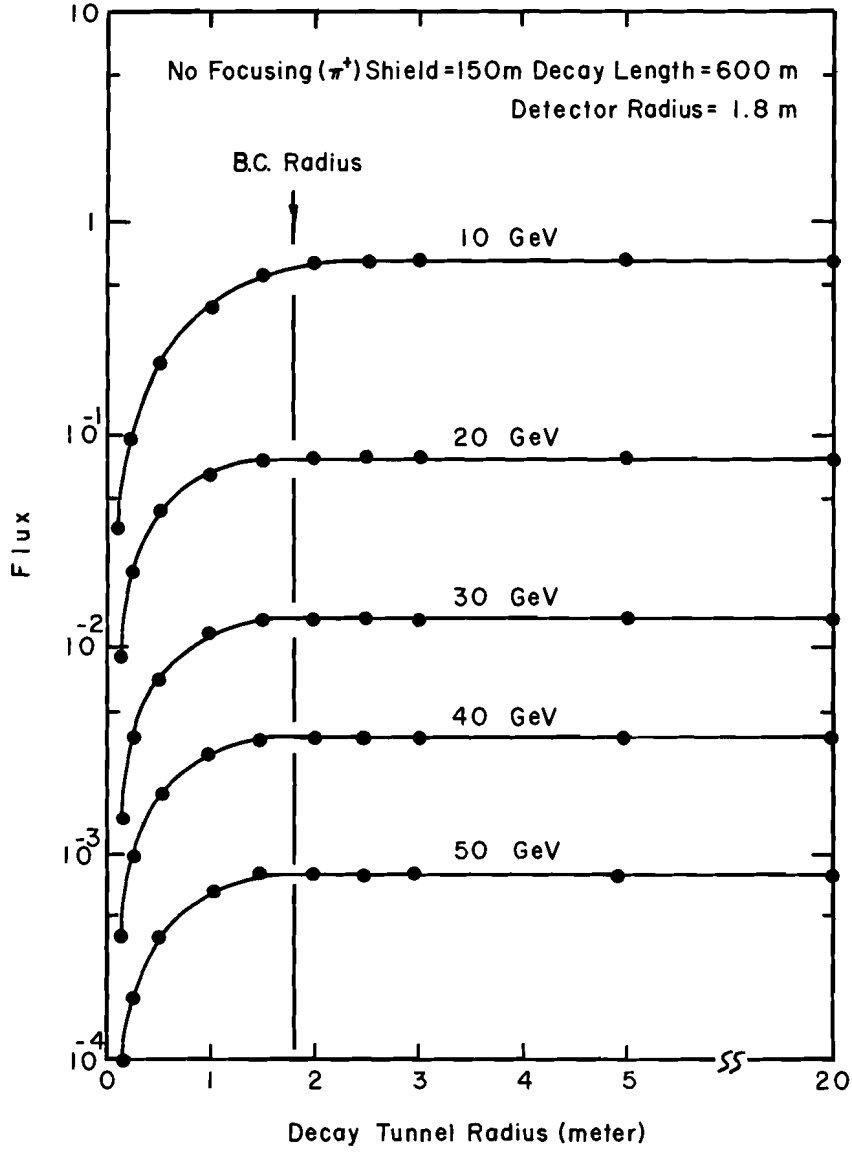

Fig. 16. The dependence on the decay tunnel radius of the neutrino flux at various energies from a non-focused pion beam.

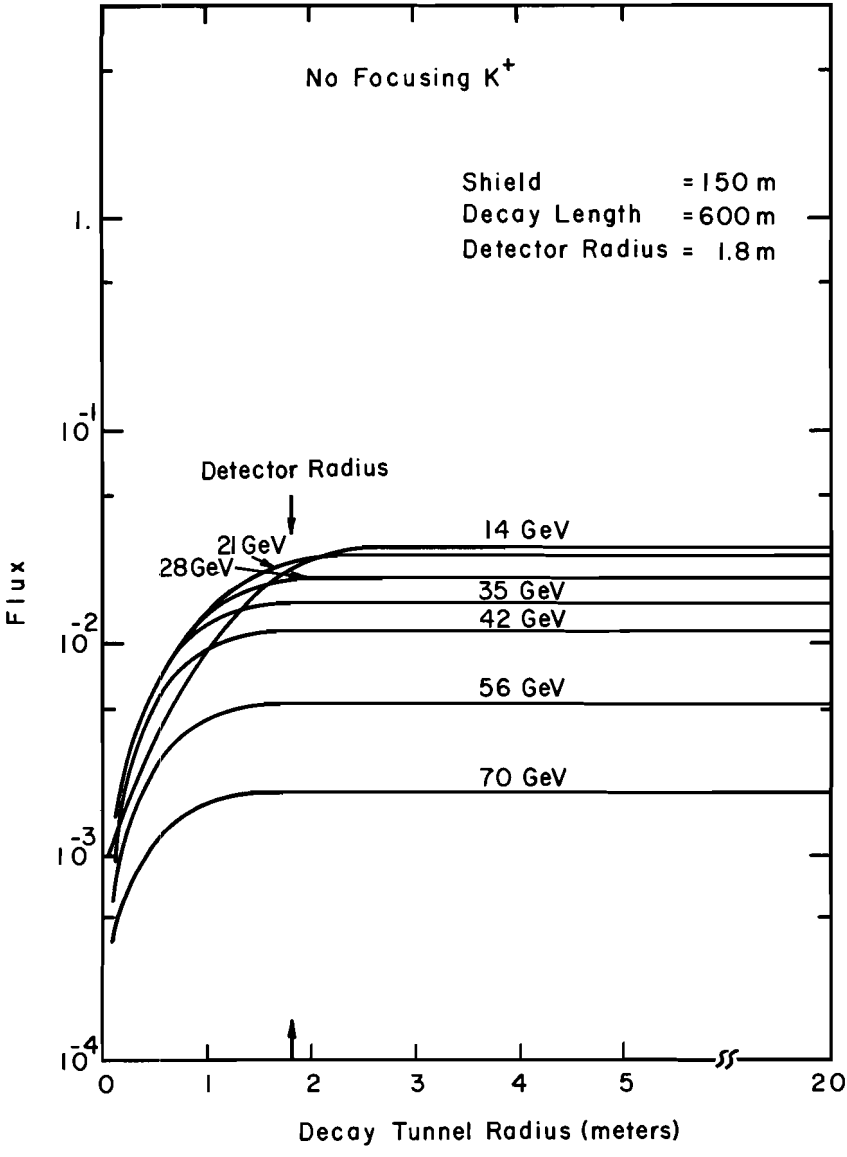

Fig. 17. The dependence of the decay tunnel radius of the neutrino flux at various energies from a non-focused kaon beam.

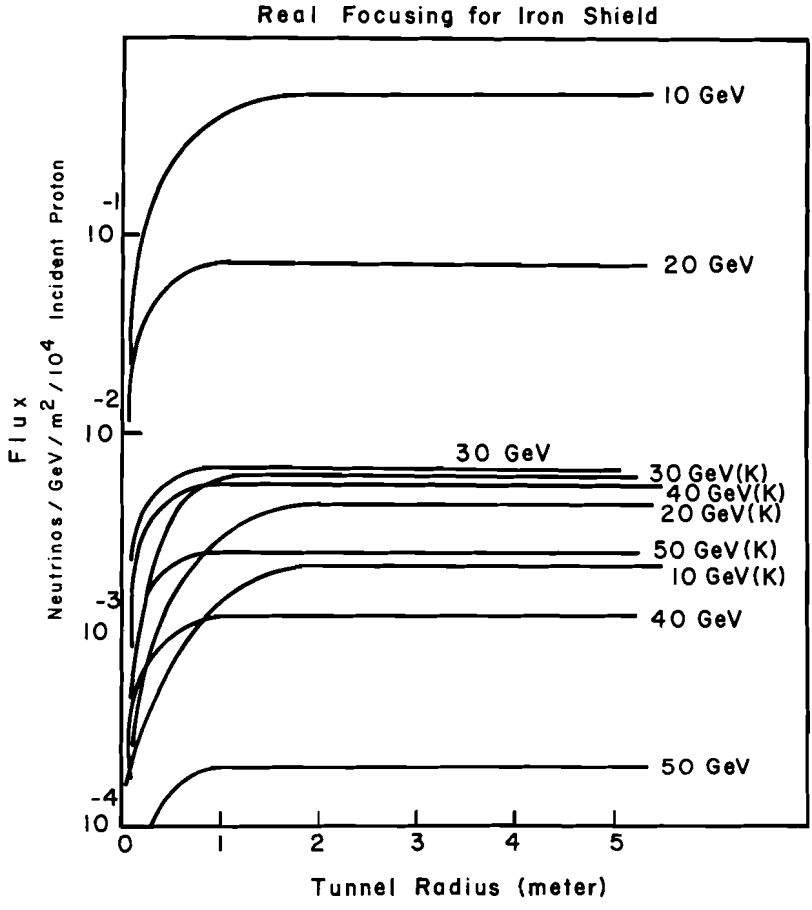

Fig. 18. The dependence on the decay tunnel radius of the neutrino flux at various energies from a real-focused pion and kaon beam.

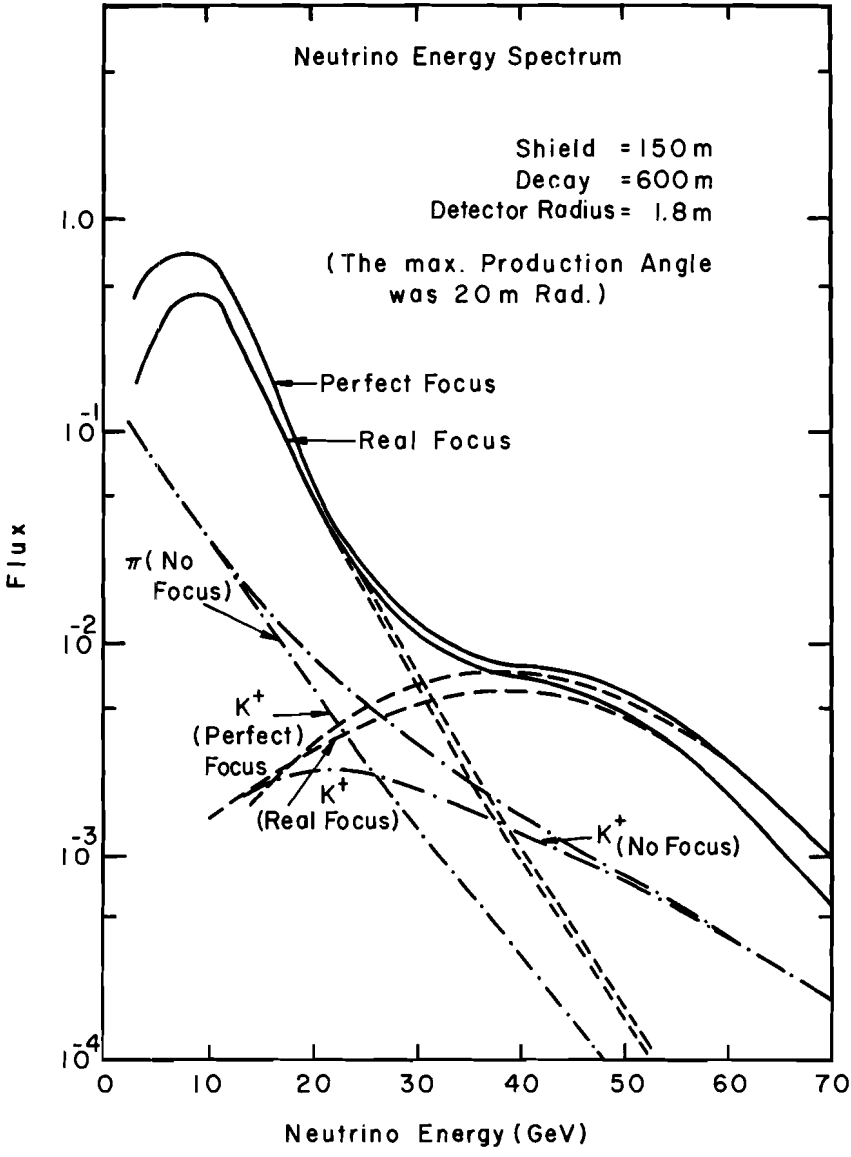

Fig. 19. The neutrino energy spectra for the iron-shielded beam for perfect, real, and no focusing.

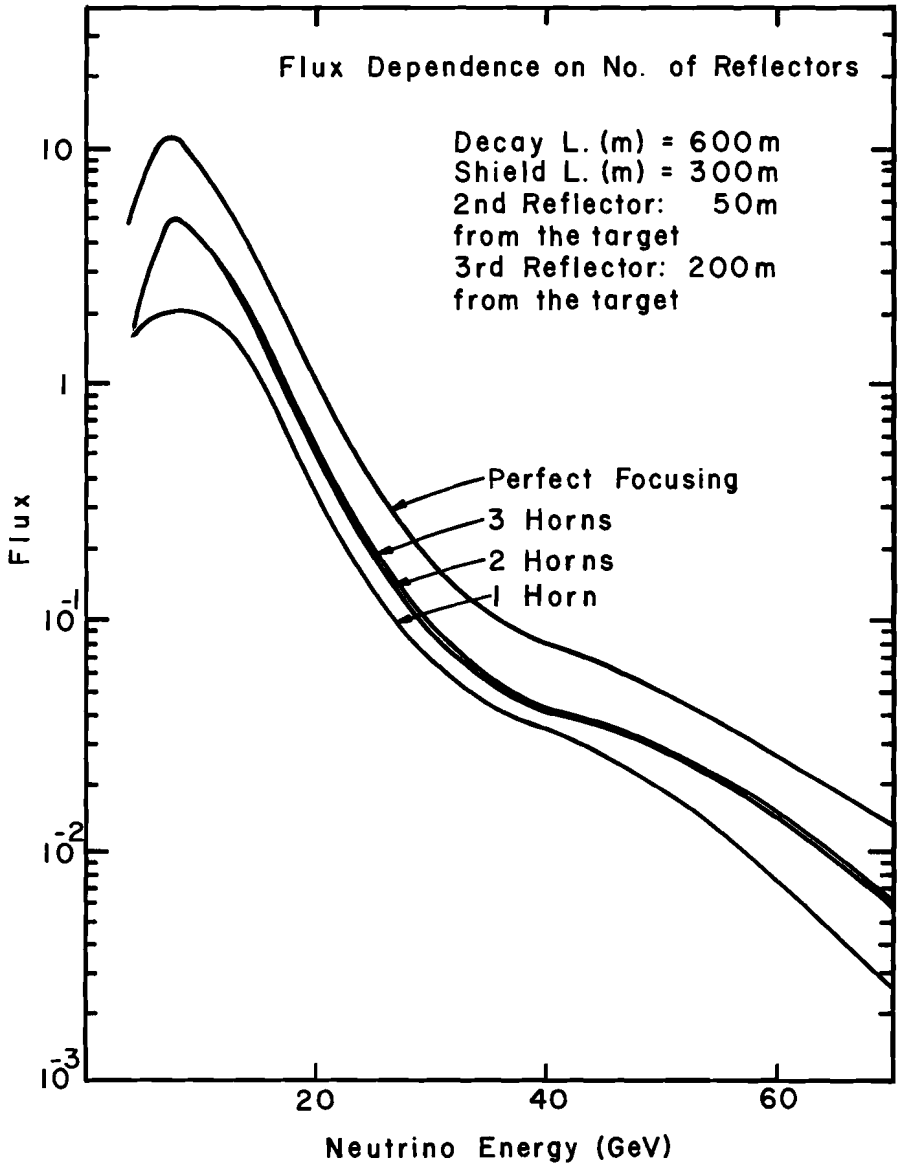

Fig. 20. The neutrino energy spectra for real-focusing systems of one, two, and three focusing elements and for a perfect-focusing system.

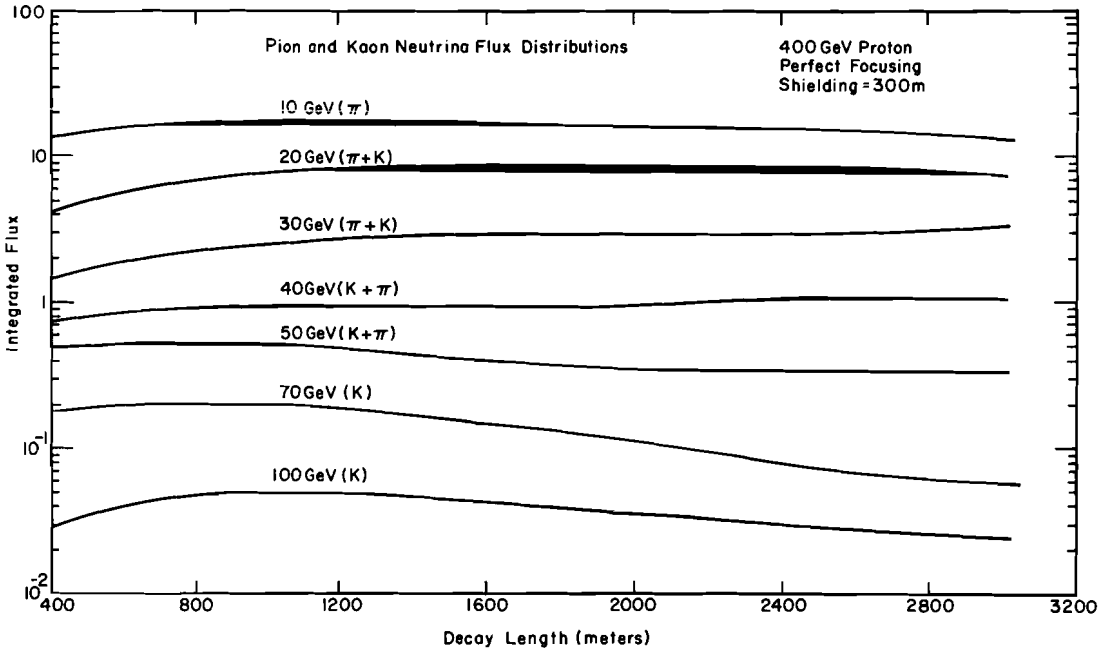

Fig. 21. The dependence of the integrated neutrino flux from pion and kaon decays on the decay length for perfect focusing at 400 GeV.

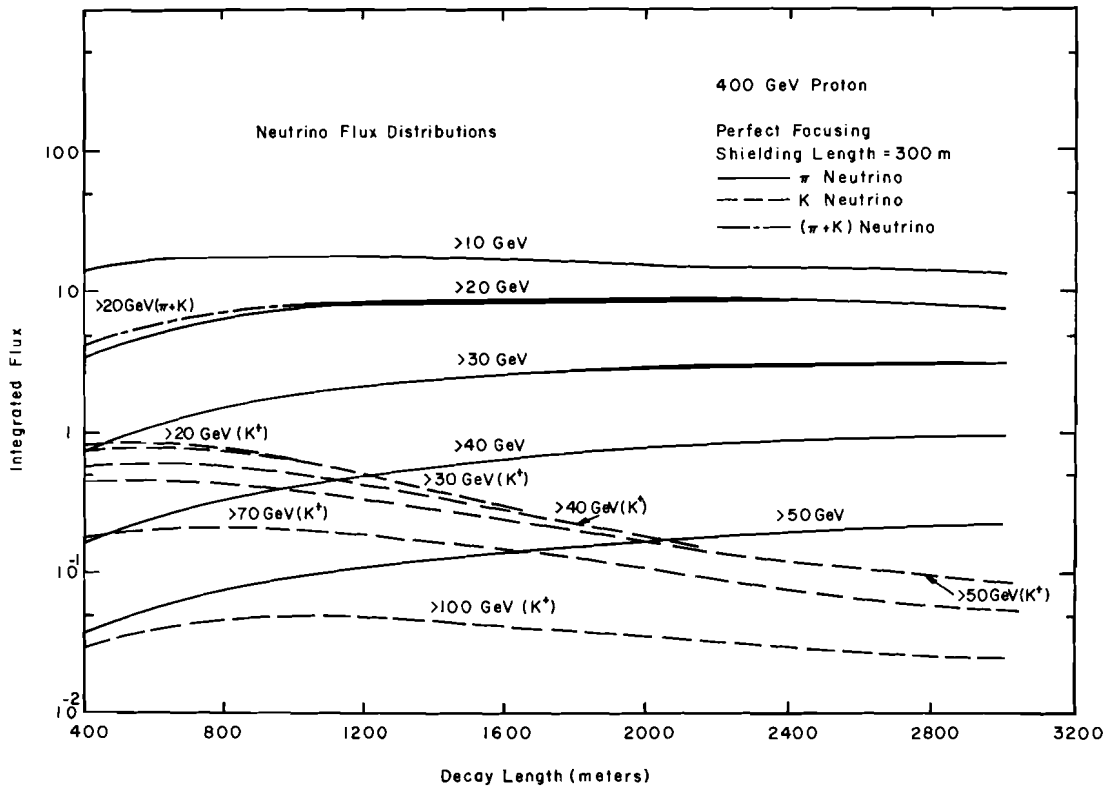

Fig. 22. The dependence of the integrated neutrino flux from pion and kaon decays individually on the decay length for perfect focusing at 400 GeV.

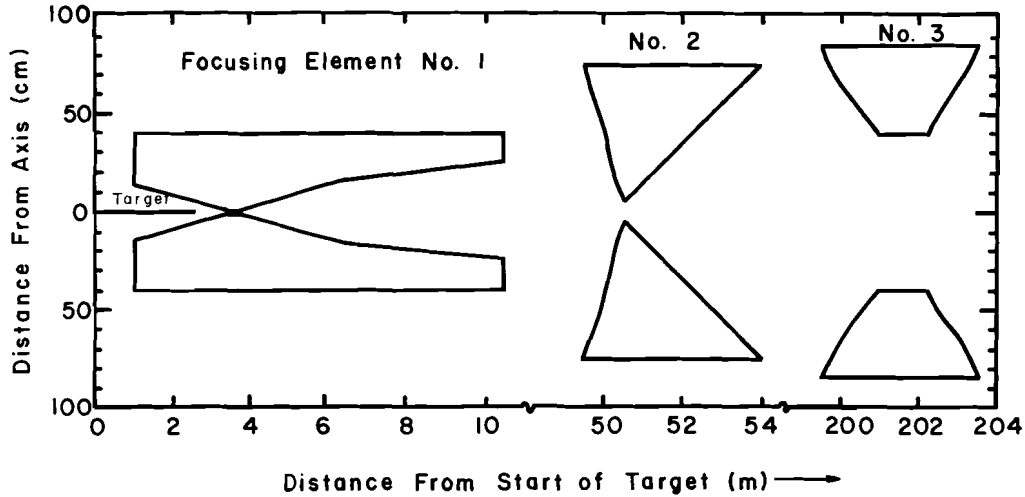

Fig. 23. The profile of the three element focusing system which optimizes the neutrino flux above 2.5 GeV passing through a detector of 1.8 m radius. The beam has a decay length of 600 m, and a shield thickness of 300 m.

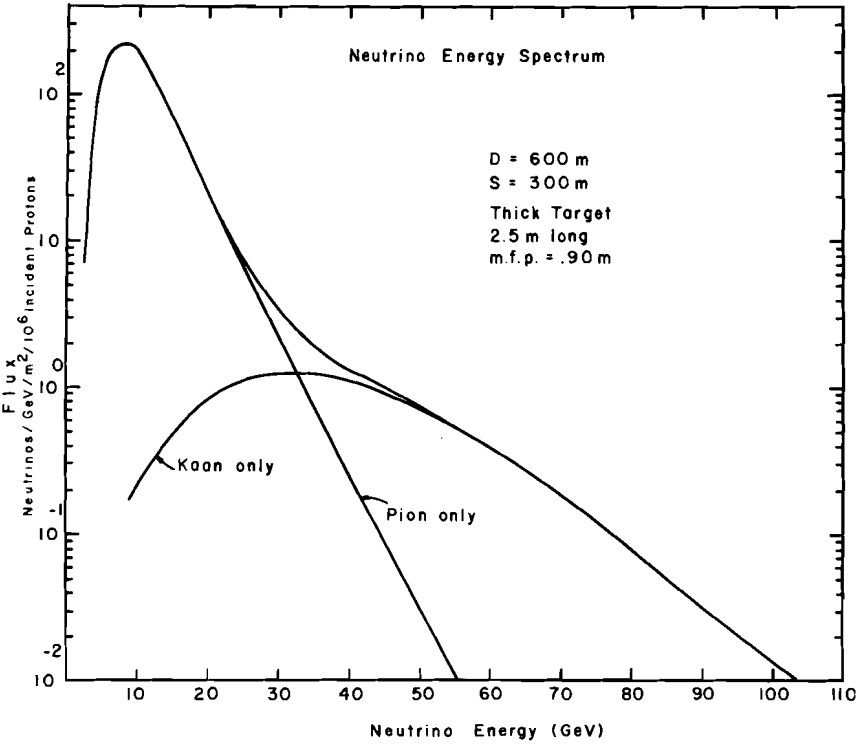

Fig. 24. The neutrino energy spectrum for the real focusing system using a 2.8 interaction length target. Attenuation in the 3 m diameter decay tunnel is not involved. This spectrum should be used for event rate calculations.

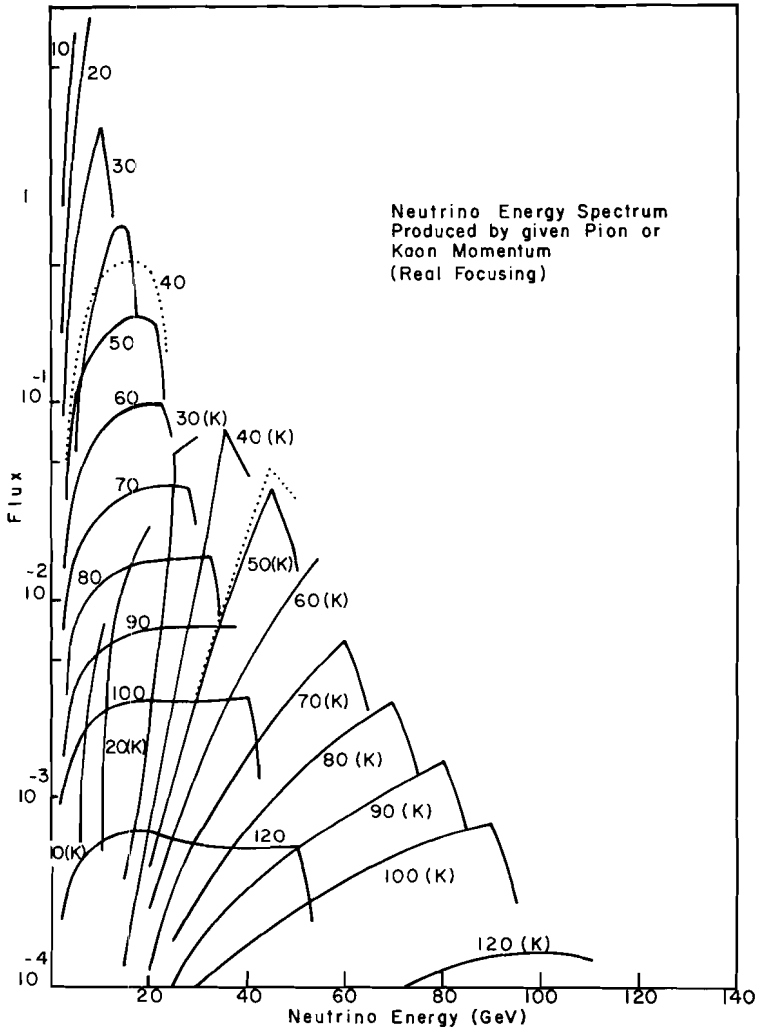

Fig. 25. The neutrino energy spectra from the decays of fixed energy parents using real focusing.